Neutron irradiation effects on gallium nitride-based Schottky diodes

Chung-Han Lin,[1] Evan J. Katz,[1] Jie Qiu,[2] Zhichun Zhang,[1] Umesh K. Mishra,[3] Lei Cao,[2] and Leonard J. Brillson[1,4,a)]
[1]*Department of Electrical and Computer Engineering, The Ohio State University, Columbus Ohio 43210, USA*
[2]*Nuclear Engineering Program, Department of Mechanical and Aerospace Engineering, The Ohio State University, Columbus, Ohio 43210 USA*
[3]*Departments of Electrical & Computer Engineering and Materials Science and Engineering, University of California, Santa Barbara, California 93106 USA*
[4]*Department of Physics and Center for Materials Research, The Ohio State University, Columbus, Ohio 43210, USA*

(Received 30 August 2013; accepted 30 September 2013; published online 16 October 2013)

Depth-resolved cathodoluminescence spectroscopy (DRCLS), time-resolved surface photovoltage spectroscopy, X-ray photoemission spectroscopy (XPS), and current-voltage measurements together show that fast versus thermal neutrons differ strongly in their electronic and morphological effects on metal-GaN Schottky diodes. Fast and thermal neutrons introduce GaN displacement damage and native point defects, while thermal neutrons also drive metallurgical reactions at metal/GaN interfaces. Defect densities exhibit a threshold neutron fluence below which thermal neutrons preferentially heal versus create new native point defects. Scanning XPS and DRCLS reveal strong fluence- and metal-dependent electronic and chemical changes near the free surface and metal interfaces that impact diode properties. © *2013 AIP Publishing LLC*. [http://dx.doi.org/10.1063/1.4826091]

The III-nitride semiconductors aluminum nitride (AlN), gallium nitride (GaN), and indium nitride (InN) have a wide range of micro- and optoelectronic applications requiring high power, and high speed. For satellite communications, these wide gap semiconductors have additional advantages of tolerance to space radiation and high temperatures. However, because satellites are subjected to high electron, proton, and bremsstrahlung radiation in earth orbit for long times, greater understanding of these radiation effects on both the semiconductor as well as its metal interfaces is needed to prevent significant electronic degradation in GaN-based platforms. In particular, high energy proton collisions generate an array of secondary particles that include neutrons with kinetic energies ranging from keV to MeV that can damage satellite circuitry by displacing atoms or generating heat. Other GaN-based device applications are also promising for nuclear reactors or in homeland security where neutrons are detected to search for special nuclear materials. Although there is extensive research on irradiation effects of GaN devices by high energy photons,[1–4] protons,[5–13] and electrons,[14–18] there is much less information on GaN devices irradiated by neutrons. Neutron irradiation can form deep levels in GaN due to displacement damage.[19–22] A collision cascade produces disordered regions and deep level traps, which can be detected by deep level transient spectroscopy, either thermally (DLTS) or optically stimulated (ODLTS),[19,20,23] thermally stimulated current (TSC) spectroscopy,[24,25] photoluminescence (PL),[3,26] and cathodoluminescence spectroscopy (CLS) techniques.[19] Under fast neutron irradiation, GaN becomes more insulating as defect states form that trap free charge. Thermal neutron irradiation may also dope GaN based on transmutation of Ga atoms to Ge.[27–29] The interplay of neutron-induced thermal, displacement, and metallurgical reaction effects is relatively unexplored, yet represents a failure mechanism for GaN aerospace and nuclear applications.

Here we report the electronic and electrical effects of neutron irradiation on GaN Schottky diodes as a function of: (1) neutron dosage, (2) fast versus thermal neutrons, and (3) defect energy level. Using a combination of depth-resolved cathodoluminescence spectroscopy (DRCLS), time-resolved surface photovoltage spectroscopy (T-SPS), and x-ray photoemission spectroscopy (XPS), we observe that neutron irradiation reduced the density of specific defects with low to medium dosage but increased their density above a threshold neutron dosage, resulting in major changes in current-voltage (I-V) characteristics. For both GaN free surfaces and metal-GaN contacts, this dosage dependence varied strongly between thermal and fast neutron irradiation.

The GaN Schottky diodes for neutron irradiation experiments were grown by metal-organic chemical vapor deposition (MOCVD). Thin film structures were grown on sapphire substrate followed by a 2 μm GaN layer doped with 3×10^{16} cm^{-3} silicon. Schottky contacts consisted of 30 nm Ni and 400 nm Au. Ohmic contacts consisted of 20 nm Ti, 150 nm Al, 40 nm Ni, and 50 nm Au, rapid thermal annealed for 30 s at 850 °C.[30] Samples were irradiated at the OSU research reactor (OSURR), a 500 kW, convection cooled, pool-type reactor with an average 5×10^{12} n/cm^2/s thermal neutron flux. A cadmium (Cd) cap filtered out thermal neutrons. Table I presents the various dosage combinations measured.

A JEOL JAMP-7800F ultrahigh vacuum (UHV) scanning electron microscope (SEM) with nanometer-scale depth resolution generated electron-hole pair excitation and cathodoluminescence spectra with electron beam energies $E_B = 2$ and 10 keV at 80 K, corresponding to peak excitation $U_0 = 25$ and 350 nm, respectively, and maximum (Bohr-Bethe) range

a)Author to whom correspondence should be addressed. Electronic mail: brillson.1@osu.edu

TABLE I. Fast and fast plus thermal neutron dosages of each GaN-metal contact.

Sample	Fast neutron fluence (n/cm^2)	Thermal neutron fluence (n/cm^2)
MOCVD1	1×10^{14}	4×10^{14}
MOCVD2	1×10^{15}	4×10^{15}
MOCVD3	1.2×10^{16}	2.8×10^{16}
MOCVD4	0	0
MOCVD5	1×10^{14}	0
MOCVD6	1×10^{15}	0
MOCVD7	1×10^{16}	0

$R_B = 75$ and 900 nm, respectively. The U_0 and R_B values were obtained by Monte Carlo simulation[31] (see supplementary material) and are consistent with GaN results with known thicknesses, e.g. (Ref. 6). A Park XE-70 atomic force microscope/Kelvin probe force microscopy (AFM/KPFM) coupled to a tungsten white light source, Oriel 260i monochromator, and optical fiber provided SPS and T-SPS spectra from GaN versus monochromatic wavelength illumination under the probe tip. An HP 4145B semiconductor parameter analyzer provided I-V characteristics.

Figures 1(a) and 1(b) show I-V characteristics of GaN Schottky diode at room temperature (T = 300 K) versus neutron fluence for (a) fast neutrons only and (b) fast plus thermal neutrons. In Fig. 1(a), there is a negligible change in reverse current for fluences up to 10^{15} n/cm^2, but a 7-fold current decrease at forward voltage $V_F = 3$ V between 10^{14} and 10^{15} n/cm^2. Both results are consistent with a decrease in free carrier density. The addition of thermal neutrons in a 4:1 ratio causes significant current changes in both forward and reverse voltage. Figure 1(b) shows 10^{15} fast plus 4×10^{15} thermal n/cm^2 produce a 20-fold decrease in forward current at $V_F = 3$ V and an order-of-magnitude increase of reverse leakage current at low voltage. Series resistance R_S from transmission line measurements increased 6.5 and 34-fold, respectively, after 1×10^{15} n/cm^2 fast and 5×10^{15} n/cm^2 fast plus thermal fluence. The nearly proportional R_S increase with neutron dose indicates both fast and thermal neutrons contribute to free carrier reduction in forward bias, whereas the increased reverse leakage current indicates increased defect densities that increase hopping and/or tunneling transport through the diode. Indeed, higher neutron fluences of 1×10^{16} n/cm^2 fast or 4×10^{16} n/cm^2 fast plus thermal irradiation both convert the Schottky barriers to ohmic contacts. The major I-V changes for neutron fluences

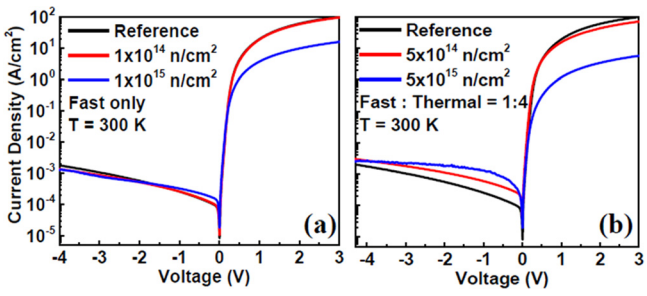

FIG. 1. (a) I-V characteristics of Schottky diodes irradiated with (a) fast and (b) fast + thermal neutron irradiation versus fluence.

$< 1\text{-}5 \times 10^{15}$ n/cm^2 suggest a threshold effect due to rates of defect formation within the GaN and/or the metal/GaN interface, which can be distinguished.

Figure 2(a) shows 2 keV low temperature (T = 80 K) DRCLS spectra in a marked GaN area between ohmic and Schottky contact before and after fast neutron irradiation. Besides the 3.45 eV near band edge emission (NBE), a 2.2 eV yellow band (YB) and 2.8–3.0 eV blue band (BB) are evident. YB emission is often associated with Ga vacancies.[32] BB emission can be associated with surface or bulk defects.[32] With 1.2×10^{16} n/cm^2 fluence, YB increases slightly, BB increases 3-fold, and the phonon replicas disappear, indicating that neutron irradiation degrades the GaN crystal lattice perfection. This degradation varies with depth. Figures 2(b) and 2(c) show magnified views of the NBE region (2.95 eV–3.75 eV) of the 2 and 10 keV DRCLS spectra, respectively. Near the free GaN surface (2 keV), the phonon replica and NBE features evident in the reference sample broaden and diminish with increasing fast as well as fast plus thermal neutron fluence. The loss of phonon replicas and NBE broadening indicate degraded crystalline quality near the surface.[33] In contrast, the GaN bulk (10 keV) spectra are relatively unchanged, indicating that GaN crystalline quality degrades strongest within 100 nm of the surface versus deeper within the bulk.

Figures 3(a) and 3(b) show the near-surface DRCLS intensity ratios I(YB)/I(NBE) and I(BB)/I(NBE) with increasing neutron fluence. YB ratios decrease 5- and 7.6-fold with initial 1×10^{14} n/cm^2 fast and 5×10^{14} n/cm^2 fast + thermal fluences. The lower minimum of fast + thermal neutrons, even with 5 times more neutrons overall, suggests that thermal effects contribute to the lower defect ratios. Indeed, while the NBE feature in Fig. 2(b) both broadens and decreases in absolute magnitude, the defect ratios decrease even further, emphasizing the thermal effect of neutrons in reducing deep level defects. Above these fluences, both ratios increase strongly above un-irradiated values. BB ratios exhibit similar behavior, decreasing 2.2- and 2.7-fold, respectively, with these initial fast and fast + thermal fluences, then increase strongly above these minimum values. For both YB and BB defect emissions, Fig. 3 shows that increasing neutron fluence first decreases then increases I(defect)/I(NBE) ratios. At all fluence levels, fast + thermal neutrons produce lower defect emissions than fast neutrons alone, indicating the thermal nature of defect reduction and the different nature of GaN interactions with fast versus thermal neutrons.

Neutrons add GaN deep level defects to those already present at different densities and rates measurable by T-SPS.[34] Figures 4(a) and 4(b) illustrate SPS spectra before and after fast (fast neutron fluence = 1×10^{16} n/cm^2) and fast + thermal neutrons (fast neutron fluence = 1.2×10^{16} n/cm^2, thermal neutron fluence = 2.8×10^{16} n/cm^2). For n-type material, the population (de-population) of deep level defect levels with electrons will increase (decrease) n-type band bending, moving Fermi level E_F lower (higher) relative to vacuum level E_{VAC} and inducing contact potential differences CPD that begin to decrease (increase) at threshold energies indicative of defect level positions E_T relative to the band edges. Thus an increasing slope indicates a photo-depopulation threshold from a level situated $E_C - E_T$ below conduction band E_C while a decreasing

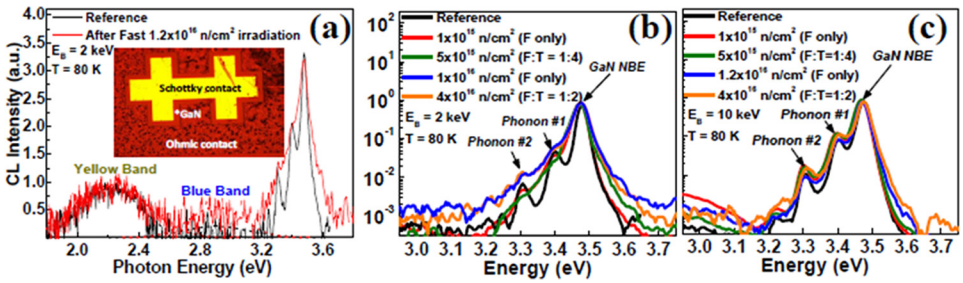

FIG. 2. (a) DRCLS spectrum at region between Schottky and ohmic contact before and after fast neutron irradiation showing 2.2 eV yellow band (YB), 2.8–3.0 blue band (BB), and 3.45 eV NBE peaks. Dashed lines are guides to the eye. Inset shows image of metal-GaN Schottky diode, ohmic contact, and bare GaN border. NBE regions probed at (b) 2 keV and (c) 10 keV show disappearance of NBE phonon replica with 10^{16} n/cm^2 in (b) but not (c).

slope indicates a photo-population threshold from the valence band E_V to a level $E_T - E_V$ above. See, e.g., Ref. 35 for a comprehensive review of SPS theory. Figure 4(a) shows a multitude of sub-gap SPS features, many of which can be paired, e.g., $E_C - 1.65$ eV depopulation and $E_V + 1.8$ eV population, as complementary transitions of the same defect level. The $E_V + 0.7$, $E_V + 0.9$, and $E_V + 1.2$ eV levels have hole traps analogs observed before and after neutron irradiation by ODLTS.[20] After neutron irradiation, Fig. 4(b) shows additional features corresponding to $E_C - 0.65$ eV and $E_V + 1.35$ eV transitions. These features are consistent with the Fig. 2(a) BB and YB emission energies, whose band gap complements are $3.45 - 2.9 = 0.55$ eV and $3.45 - 2.2 = 1.25$ eV, respectively, notwithstanding Frank–Condon shifts. These additional features appear as more pronounced slope changes near pre-irradiation CPD features, reflecting an increase in already existing defects as well as creation of new defect types.

We used T-SPS to distinguish between these defects by their densities and evolution versus neutron fluence. The density n_t^0 of each defect level for a given threshold hυ and flux can be estimated from

$$n_t^0 = -\frac{40\dot{V}_S^0 \delta V_S^1}{2\dot{V}_S^1 \sqrt{|V_S^0|}\left(1 + \frac{\dot{V}_S^0}{\dot{V}_S^1}\right)} \sqrt{\frac{2\epsilon\epsilon_0 k_B T N_B}{q^2}}, \quad (1)$$

for Boltzmann constant k_B, temperature T, dielectric constant ϵ, free space permittivity ϵ_0, bulk doping density N_B. The factor of 40 is the normalization factor of $1/k_BT$. CPD slope change $\dot{V}_S^0$ when light turns on, CPD slope change $\dot{V}_S^1$ when light turns off, surface potential CPD V_S^0 without light in dimensionless units (normalized to kT/q), saturated and normalized CPD V_S^1 with light on, and $\delta V_S^1 = V_S^1 - V_S^0$.[34,36,37]

Figures 5(a) and 5(b) display surface densities obtained from T-SPS versus fast and fast + thermal neutron fluences, respectively. The highest density defects in Fig. 5(a), $E_V + 1.2$ eV, $E_C - 1.1$ eV, and $E_C - 1.65$ eV, show decreases at 1×10^{14} n/cm^2 fluence followed by increases at higher fluences analogous to I(defect)/I(NBE) ratios in Fig. 3. These levels are also the closest to mid-gap so that they are most effective at carrier recombination across the band gap. The $E_V + 1.2$ eV defect exceeds other defect densities by nearly an order of magnitude and correlates closest to the YB transition observed in DRCLS.

The corresponding bulk density of this dominant $E_V + 1.2$ eV defect can be estimated from Fig. 5(a) using the surface depletion width W since photogenerated free carriers require an electric field in order to drift and change surface potentials.[34] From Poisson's equation

$$W = \sqrt{\frac{2\epsilon\epsilon_0 \times V_{bi}}{qN_b}}, \quad (2)$$

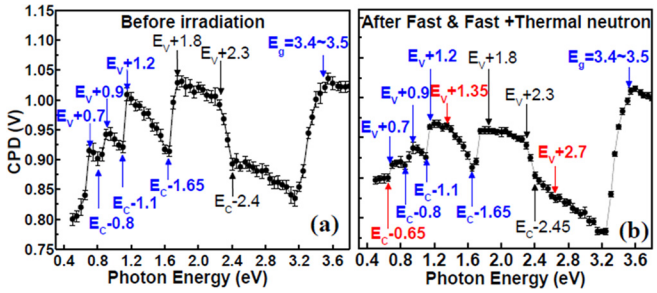

FIG. 4. SPS spectra at region between Schottky and ohmic contact (a) before and (b) after fast or fast + thermal neutron irradiation. Energy levels in red are defect features appearing after neutron irradiation.

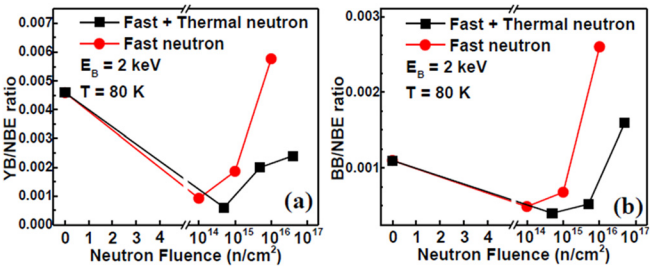

FIG. 3. DRCLS intensity ratio (a) I(YB)/I(NBE) and (b) I(BB)/I(NBE) variation with neutron fluence. Ratio decreases with intermediate fluence signify improved crystal quality. Ratio increases at higher fluences can account for deterioration in I-V rectification with fluence.

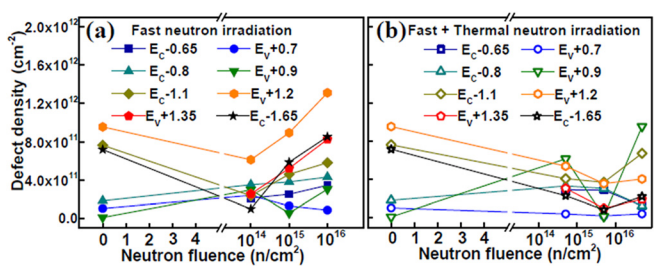

FIG. 5. The evolution of defect densities with (a) fast and (b) fast + thermal neutron irradiatin. Defect decreases in (a) are similar to those in Fig. 3. Lower densities in (b) are consistent with thermal defect healing at low fluences.

and an estimated band bending $V_{bi} = 1\,eV$, $W = 0.18 \times 10^{-4}\,cm$. The corresponding change in bulk density is $0.35 \times 10^{12}\,cm^{-2} / 0.18 \times 10^{-4}\,cm = 1.94 \times 10^{16}$ new defects cm^{-3}, corresponding to an introduction rate of $1.94\,cm^{-1}$ for $10^{16}\,n/cm^2$ fluence. This is quite close to the $1.9\,cm^{-1}$ introduction rate typical of many traps, e.g., an MOCVD -grown GaN sample with $3.8 \times 10^{16}\,cm^{-3}$ doping and $2 \times 10^{16}\,n/cm^2$ fast neutron fluence reported previously for traps with 0.45 eV activation energy.[20] Introduction rates of 1.89, 1.38, 1.62, 4.55, and $0.75\,cm^{-1}$ were calculated for $E_C - 0.65$, $E_C - 0.8$, $E_V + 0.9$, $E_V + 1.35$, and $E_C - 1.65$ transitions, respectively. In contrast, densities measured for fast + thermal neutrons in Fig. 5(b) all decreased with the exception of $E_V + 0.9\,eV$ defects, again showing that additional thermal neutrons act to suppress or "heal" some defects created by fast neutrons. It should be mentioned here that the n_t/W estimation is based on the transient surface photovoltage change in surface charge. The width of the surface depletion region is a first-order estimate of the depth over which photoexcited charge can move to/away from the surface and influence the contact potential. It assumes photoexcitation depth extends at least throughout the depletion width and that the transient occurs over times longer than time for charge to diffuse to/away from the surface.

Fast + thermal neutrons also produce metallurgical reactions at metal-GaN interfaces. Figure 6(a) shows XPS spectra for 40 nm Ni films on GaN (1) before (smooth surface SEM) and (2) after $1 \times 10^{16}\,n/cm^2$ fast + thermal neutron fluence (mottled, i.e., melted, surface SEM). Spectra show the Ni core level signals in both and the appearance of Ga with the Ni in the mottled areas of (2), indicating interdiffusion. No such mottling appears for fast neutrons only. Similarly, Figs. 6(b) and 6(c) show SEM micrographs, respectively, of 40 nm Ti films on GaN before (smooth) and after (pinwheels and bubbles) the same fluence. Again, fast neutrons alone produce no such features. Ni-GaN interdiffusion occurs at temperature around 300 °C–400 °C[38,39] and nitrogen diffusion into Ti layer begins at ~500 °C,[40] forming needle crystallites and bubbles patterns[41] similar to Fig. 6(c). The appearance of these morphological changes demonstrates that temperatures reach at least a few hundred degrees at metal-GaN interfaces during exposure to $5 \times 10^{12}\,n/cm^2/s$ neutron fluxes. Such temperatures are difficult to measure during irradiation since, as Fig. 2 shows, defect formation is localized to within a few hundred nanometers of the GaN surface. Therefore, the variation of GaN defect densities after fast + thermal neutron irradiation and the deterioration of GaN Schottky diode I-V characteristics may be due to a combination of a local thermal spike that reduces defect densities of GaN and enhanced metal-GaN interdiffusion that creates new interface defects. The appearance of Ga in the Ni overlayer indicates that Ga vacancies (V_{Ga}) form. Indeed, the V_{Ga} signature is the YB emission at $E_V + 1.2\,eV$,[32] whose density dominates all other defects in Fig. 5(a).

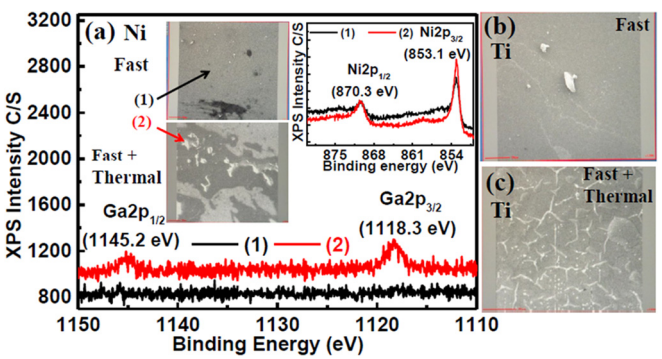

FIG. 6. (a) XPS spectra of a 40 nm Ni/GaN sample (1) after fast neutron and (2) fast + thermal neutron irradiation. SEM maps (inset) display (1) smooth Ni films with fast versus (2) mottled overlayer after fast + thermal irradiation. Analogous SEM maps for 40 nm Ti/GaN after (b) fast and (c) fast + thermal radiation. Different surface morphologies between (a) and (c) show that fast + thermal neutrons interact with Ti and Ni metal differently.

Fast neutrons also exhibit density decreases with $1 \times 10^{14}\,n/cm^2$ fast neutrons, which can be attributed to GaN recrystallization.[42] Higher fluences offset this defect reduction by displacement damage or lattice disorder created by primary knock-on atoms due to high energy neutron collisions. Increases of the $E_C - 1.1\,eV$ defect density can be related to N interstitials,[21,23,24] $E_V + 1.2\,eV$ increases to V_{Ga} formation[32] and both $E_C - 0.65\,eV$ and $E_V + 1.35\,eV$ increase to edge dislocations[43] or lattice disorder. Increase of the $E_C - 0.8\,eV$ defect density supports the presence of lattice disorder,[21,23] while the $E_C - 0.65\,eV$ level is associated with large Frank-Condon shifts and lattice relaxation.[22]

In summary, our results show that Schottky barrier I-V characteristics are strongly affected by fast and fast + thermal neutron irradiation. The different effects of fast and thermal neutrons are due to a competition between lattice displacement damage that produces native point defects versus thermally induced defect "healing" at intermediate fluences that can improve crystal quality. A threshold effect is apparent for both fast and thermal neutrons between 10^{14} and $10^{15}\,n/cm^2$ fluences. The preferential near-surface defect formation points to localized surface heating by thermal neutrons to temperatures not easily measured macroscopically. Besides lattice annealing, thermal neutrons induce chemical interdiffusion and morphology changes, which in turn disrupt metal-GaN Schottky barriers. Optimizing Schottky contact resistance to neutron irradiation requires taking both these displacement and thermal effects into account.

The authors wish to thank the staff at the Ohio State University Nuclear Reactor Laboratory for their support. This research was performed with support from the Department of Energy Office of Nuclear Energy's Nuclear Energy University Programs, the Office of Naval Research DRIFT MURI under Grant No. N00014-08-1-0655 (Dr. Paul Maki and Harry Dietrich), and a facility grant from The Ohio State University Institute for Materials Research.

[1]G. A. Umana-Membereno, J. M. Dell, G. Parish, B. D. Nener, L. Faraone, and U. K. Mishra, IEEE Trans. Electron Devices **50**, 2326 (2003).
[2]B. Luo, J. W. Johnson, F. Ren, K. K. Allums, C. R. Abernathy, S. J. Pearton, A. M. Dabiran, A. M. Wowchack, C. J. Polley, P. P. Chow, D. Schoenfeld, and A. G. Baca, Appl. Phys. Lett. **80**, 604 (2002).
[3]E. Gaubas, K. Kazlauskas, J. Vaitkus, and A. Žukauskas, Phys. Status Solidi C **2**, 2429 (2005).
[4]O. Aktas, A. Kuliev, V. Kumar, R. Schwindt, S. Toshkov, D. Costescu, J. Stubbins, and I. Adesida, Solid-State Electron. **48**, 471 (2004).
[5]A. P. Karmarkar, B. Jun, D. M. Fleetwood, R. D. Schrimpf, R. A. Weller, B. D. White, L. J. Brillson, and U. K. Mishra, IEEE Trans. Nuclear Sci. **51**, 3801 (2004).

[6]B. D. White, M. Bataiev, S. H. Goss, X. Hu, A. Karmarkar, D. M. Fleetwood, R. D. Schrimpf, W. J. Schaff, and L. J. Brillson, IEEE Trans. Nucl. Sci. **50**, 1934 (2003).
[7]X. Hu, B. K. Choi, H. J. Barnaby, D. F. Fleetwood, R. D. Schrimpf, S. Lee, S. Shojah-Ardalan, R. Wilkins, U. K. Mishra, and R. W. Dettmer, IEEE Trans. Nucl. Sci. **51**, 293 (2004).
[8]X. Hu, A. P. Karmarkar, B. Jun, D. M. Fleetwood, R. D. Schrimpf, R. D. Geil, R. A. Weller, B. D. White, M. Bataiev, L. J. Brillson, and U. K. Mishra, IEEE Trans. Nucl. Sci. **50**, 1791 (2003).
[9]F. Gaudreau, P. Fournier, C. Carlone, S. M. Khanna, H. Tang, J. Webb, and A. Houdayer, IEEE Trans. Nucl. Sci. **49**, 2702 (2002).
[10]B. D. White, M. Bataiev, L. J. Brillson, B. K. Choi, D. M. Fleetwood, R. D. Schrimpf, S. T. Pantelides, R. W. Dettmer, W. J. Schaff, J. G. Champlain, and U. K. Mishra, IEEE Trans. Nucl. Sci. **49**, 2695 (2002).
[11]B. Luo, J. W. Johnson, F. Ren, K. K. Allums, C. R. Abernathy, S. J. Pearton, R. Dwivedi, T. N. Fogarty, R. Wilkins, A. M. Dabiran, A. M. Wowchack, C. J. Polley, P. P. Chow, and A. G. Baca, J. Electron. Mater. **31**, 437 (2002).
[12]F. D. Auret, S. A. Goodman, F. K. Koschnick, J.-M. Spaeth, B. Beaumont, and P. Gibart, Appl. Phys. Lett. **74**, 407 (1999).
[13]A. Y. Polyakov, A. S. Usikov, B. Theys, N. B. Smirnov, A. V. Govorkov, F. Jomard, N. M. Shmidt, and W. V. Lundin, Solid-State Electron. **44**, 1971 (2000).
[14]L. Polenta, Z.-Q. Fang, and D. C. Look, Appl. Phys. Lett. **76**, 2086 (2000).
[15]A. Y. Polyakov, I.-H. Lee, N. B. Smirnov, A. V. Govorkov, E. A. Kozhukhova, N. G. Kolin, A. V. Korulin, V. M. Boiko, and S. J. Pearton, J. Appl. Phys. **109**, 123703 (2011).
[16]A. Ionascut-Nedelcescu, C. Carlone, A. Houdayer, H. J. von Bardeleben, J.-L. Cantin, and S. Raymond, IEEE Trans. Nucl. Sci. **49**, 2733 (2002).
[17]D. C. Look, D. C. Reynolds, J. W. Hemsky, J. R. Sizeolove, R. L. Jones, and R. J. Molnar, Phys. Rev. Lett. **79**, 2273 (1997).
[18]H. Nykänen, S. Suihkonen, L. Kilanski, M. Sopanen, and F. Tuomisto, Appl. Phys. Lett. **100**, 122105 (2012).
[19]A. Y. Polyakov, N. B. Smirnov, A. V. Govorkov, A. V. Markov, S. J. Pearton, N. G. Kilin, D. I. Merkurisov, V. M. Boiko, C.-R. Lee, and I.-H. Lee, J. Vac. Sci. Technol. B **25**, 436 (2007).
[20]I.-H. Lee, A. Y. Polyakov, N. B. Smirnov, A. V. Govorkov, E. A. Kozhukhova, N. G. Kolin, V. M. Korulin, and S. J. Pearton, J. Electrochem. Soc. **158**, H866 (2011).
[21]A. Y. Polyakov, N. B. Smirnov, A. V. Govorkov, A. V. Markov, N. G. Kolin, D. I. Merkurisov, V. M. Boiko, K. D. Shcherbatchev, V. T. Bublik, M. I. Voronova, I.-H. Lee, C. R. Lee, S. J. Pearton, A. Dabirian, and A. V. Osinsky, J. Appl. Phys. **100**, 093715 (2006).
[22]S. Li, J. D. Zhang, C. D. Beling, K. Wang, R. X. Wang, M. Gong, and C. K. Sarkar, J. Appl. Phys. **98**, 093517-1 (2005).
[23]A. Y. Polyakov, S. J. Pearton, P. Frenzer, F. Ren, L. Liu, and J. Kim, J. Mater. Chem. C **1**, 877 (2013).
[24]K. Kuriyama, M. Ooi, A. Onoue, K. Kushida, M. Okada, and Q. Xu, Appl. Phys. Lett. **88**, 132109 (2006).
[25]M. Zhang, X. Wang, H. Xiao, C. Yang, and R. Wang, in IEEE International Conference on Solid-State and Integrated Circuit Technology (ICSICT, Shanghai), November 2010.
[26]R. X. Wang, S. J. Xu, S. Fung, C. D. Beling, K. Wang, S. Li, Z. F. Wei, T. J. Zhou, J. D. Zhang, and Y. Huang, Appl. Phys. Lett. **87**, 031906 (2005).
[27]A. Y. Polyakov, N. B. Smirnov, A. V. Govorkov, N. G. Kolin, D. I. Merkurisov, V. M. Boiko, A. V. Korulin, and S. J. Pearton, J. Vac. Sci. Technol. B **28**, 608 (2010).
[28]I.-H. Lee, A. Y. Polyakov, N. B. Smirnov, A. V. Govorkov, E. A. Kozhukhova, E. B. Yakimov, N. G. Kolin, V. M. Boiko, A. V. Korulin, and S. J. Pearton, Appl. Phys. Lett. **98**, 212107 (2011).
[29]K. Kuriyama, T. Tokumasu, J. Takahashi, H. Kondo, and M. Okada, Appl. Phys. Lett. **80**, 3328 (2002).
[30]A. P. Karmakar, B. D. White, D. Buttari, D. M. Fleetwood, R. D. Schrimpf, R. A. Weller, L. J. Brillson, and U. K. Mishra, IEEE Trans. Nucl. Sci. **52**, 2239 (2005).
[31]P. Hovington, R. Gauvin, A. R. Couture, D. Drouin, P. Horny, and H. Demers, CASINO version 2.42, Monte Carlo simulation of electron trajectory in solids, 2002; See supplementary material at http://dx.doi.org/10.1063/1.4826091 for GaN Monte Carlo simulation.
[32]M. A. Reshchikov and H. Morkoç, J. Appl. Phys. **97**, 061301 (2005).
[33]M. A. Rechchikov, D. Huang, F. Yun, P. Visconti, L. He, H. Morkoc, J. Jasinski, Z. Liliental-Weber, R. J. Monlnar, S. S. Park, and K. Y. Lee, J. Appl. Phys. **94**, 5623 (2003).
[34]Z. Zhang, V. Quemener, C.-H. Lin, B. G. Svensson, and L. J. Brillson, Appl. Phys. Lett. **103**, 072107 (2013).
[35]L. Kronik and Y. Shapira, Surf. Sci. Rep. **37**, 1 (1999).
[36]J. Lagowski, C. L. Balestra, and H. C. Gatos, Surf. Sci **29**, 203 (1972).
[37]L. J. Brillson, Surf. Sci **69**, 62 (1977).
[38]J. D. Guo, F. M. Pan, M. S. Feng, R. J. Guo, P. F. Chou, and C. Y. Chang, J. Appl. Phys. **80**, 1623 (1996).
[39]A. Barinov, L. Gregoratti, B. Kaulich, M. Kiskinova, and A. Rizzi, Appl. Phys. Lett. **79**, 2752 (2001).
[40]C. L. Lu, A. V. Davydon, D. Josell, and L. A. Bendersky, J. Appl. Phys. **94**, 245 (2003).
[41]Y. L. Jeyachanfran, S. K. Narayandass, D. Mangalaraj, S. Areva, and J. A. Mielczarski, Mater. Sci. Eng. A. **445–446**, 223 (2007).
[42]C.-W. Wang, J. Vac. Sci. Technol. B **20**, 1821 (2002).
[43]D. Johnstone, Proc. SPIE **6473**, 64730L (2007).